Published in final edited form as:
Phys Chem Chem Phys. 2012 September 21; 14(35): 12355–12367. doi:10.1039/c2cp41291h.

New insights into the electrochemical desorption of alkanethiol SAMs on gold

Evangelina Pensa[a], **Carolina Vericat**[a], **Doris Grumelli**[a], **Roberto C. Salvarezza**[a], **Sung Hyun Park**[b,c], **Gabriel S. Longo**[c,d], **Igal Szleifer**[b,c], and **Lucila P. Méndez De Leo**[e]

Lucila P. Méndez De Leo: lmendezdeleo@qi.fcen.uba.ar

[a]Instituto de Investigaciones Fisicoquímicas Teóricas y Aplicadas (INIFTA- CONICET- CCT La Plata), 1900 La Plata, Buenos Aires, Argentina.

[b]Department of Biomedical Engineering, Northwestern University, Evanston, Illinois 60208, U.S.A.

[c]Chemistry of Life Processes Institute, Northwestern University, Evanston, Illinois 60208, U.S.A.

[d]Department of Materials Science and Engineering, Northwestern University, Evanston, Illinois 60208, U.S.A.

[e]INQUIMAE, CONICET, DQIAQF, FCEN, UBA, Ciudad Universitaria, Pabellón II. Buenos Aires, Argentina.

Abstract

A combination of Polarization Modulation Infrared Reflection Absorption Spectroscopy (PMIRRAS) under electrochemical control, Electrochemical Scanning Tunneling Microscopy (ECSTM) and Molecular Dynamics (MD) simulations has been used to shed light on the reductive desorption process of dodecanethiol (C12) and octadecanethiol (C18) SAMs on gold in aqueous electrolytes. Experimental PMIRRAS, ECSTM and MD simulations data for C12 desorption are consistent with formation of randomly distributed micellar aggregates stabilized by Na^+ ions, coexisting with a lying-down phase of molecules. The analysis of pit and Au island coverage before and after desorption is consistent with the thiolate-Au adatoms models. On the other hand, PMIRRAS and MD data for C18 indicate that the desorbed alkanethiolates adopt a Na^+ ion-stabilized bilayer of interdigitated alkanethiolates, with no evidence of lying down molecules. MD simulations also show that both the degree of order and tilt angle of the desorbed alkanethiolates change with the surface charge on the metal, going from bilayers to micelles. These results demonstrate the complexity of the alkanethiol desorption in the presence of water and the fact that chain length and counterions play a key role in a complex structure.

Introduction

Self assembled monolayers (SAMs) of alkanethiols ($CH_3(CH_2)_nSH$) on metals and semiconductors are of great interest from a fundamental point of view and due to their multiple nanotechnological applications.[1] In particular, alkanethiol SAMs on gold (and especially on the (111) surface) have been regarded as a model system for the study of these two-dimensional structures. In addition to the many studies found in the literature on the structure and the arrangement of the thiol molecules on the surface, the stability of SAMs under various conditions and the dynamics of the adsorption and desorption processes have

Correspondence to: Lucila P. Méndez De Leo, lmendezdeleo@qi.fcen.uba.ar.

been studied by many different groups with a myriad of physical chemical techniques. However, several questions remain unanswered[1,2] and, in recent years, there has been a renewed interest in the understanding of these apparently simple systems.

Upon adsorption, alkanethiols with a number of C atoms n>1 first form low-coverage, lying-down structures (striped phases) on Au(111) and then arrange in the √3×√3 R30° lattice and its related c(4×2) superlattice with coverage θ=0.33.[1,3] Chemisorbed molecules show a tilt angle α between the surface normal and the hydrocarbon chain. However, an important discussion is being held at present in the surface science community regarding the actual structure of these two high coverage lattices in the frame of some experimental evidence about the existence of a strong reconstruction of the Au(111) surface that involves gold adatom formation.[2] These adatoms are provided in part by the lifting of the 22×√3 Au(111) reconstruction and, mainly, through the formation of vacancy islands ("pits") on the (111) terraces.[1] Several models have been proposed that involve the existence of some kind of RS-Au or $(RS)_2$-Au units at the interface (where RS- stands for chemisorbed thiol), with or without single gold vacancies.[1,4–7] While models involving RS-Au species can describe both √3×√3 R30° and c(4×2) lattices, the proposed models based on $(RS)_2$-Au species (which happen to be energetically more favoured) are strictly applicable only to c(4×2) lattices.[2]

Adatom models have obtained some experimental support from the analysis of the surface coverage of pits (θ_{pits}) and also from that of gold islands formed after SAM desorption (θ_{isl}), since the latter are thought to be formed by nucleation of released Au adatoms from the RS-Au or $(RS)_2$-Au species.[8,9] While some of these studies have been performed in vacuum (either induced by temperature or by exposure to atomic hydrogen), SAM desorption at a water/Au interface is more complex due to the low solubility of alkanethiols in aqueous environments, where they can form different kinds of surface structures. In this context, recent Scanning Tunneling Microscopy (STM) results in moist air of the desorption of alkanethiol SAMs on Au(111) induced by the tip showed a θ_{isl} compatible with a RS-Au model.[9] It was there assumed that complete desorption of thiolates takes place, i. e., the observed islands are only formed by gold atoms, with no contribution of thiol species in the structures, in contrast with previous electrochemical STM (ECSTM) results.[10]

Therefore, elucidation of the surface structures formed after thiol desorption in liquids is an interesting point not only to contribute to the knowledge of the desorption mechanism, but also to validate the information obtained by STM related to the structure of the Au(111) surface after thiol desorption, particularly for intermediate and long thiols, where the dominant √3×√3 R30° lattice remains controversial.

Although the reductive desorption pathway and the different structures formed on the Au(111) surface have been already studied by several techniques, including STM and ECSTM, force curve measurements by electrochemical Atomic Force Microscopy (ECAFM)[11] and IR[10,12–16], no clear conclusions can be drawn from the analysis of the previous studies. In fact, the observed features have been attributed both to gold islands[17,18] and to the formation of disordered molecular aggregates or micelles[10,11,15,16], depending on both the experimental techniques used to analyze the system and the alkanethiol chain length.

In this work, the combination of Polarization-Modulation InfraRed Reflection-Absorption Spectroscopy (PMIRRAS), STM under electrochemical control and Molecular Dynamics (MD) simulations have been used to shed light on the reductive desorption process of dodecanethiol (C12) and octadecanethiol (C18) SAMs on gold. We provide evidence that the structures observed *in situ* for C12 desorption in aqueous electrolytes on the Au surface

are not simple Au islands. Only after a careful ex situ cleaning procedure the Au islands can be observed. In contrast to previous data, the pit coverage and island coverage support the presence of $(RS)_2$-Au species in the $\sqrt{3}\times\sqrt{3}$ R30° lattice. The experimental data and MD simulations indicate that the C12 micelles are surrounded by lying down molecules and stabilized by Na^+ ions. On the other hand, for C18 a Na^+ ion-stabilized bilayer of interdigitated alkanethiolates becomes dominant on the Au surface. MD simulations indicate that the degree of order and tilt angle of the hydrocarbon chains change with desorption potential, so that formation of micelles or bilayers can be "tuned" by changing the potential applied to the interface. While we cannot unambiguously demonstrate the presence of Au adatoms incorporated into the micelles, it is evident that the structures imaged by STM in aqueous electrolyte cannot be described as simple Au islands, thus opening a question about the interpretation of tip-induced thiol desorption in moist air and pointing out the crucial role of the chain length and of the counterions in the process.

Experimental Section

Chemicals

1-dodecanethiol (C12) (≥98%), 1-octadecanethiol (C18) (98%) and sodium hydroxide were used as received (Aldrich Chemical Co. Milwaukee, WI). Absolute ethanol, MilliQ® water and deuterated water 99.9 % (Aldrich Chemical Co. Milwaukee, WI) were used as solvents.

Electrode Preparation

The PMIRRAS electrode is a gold disk that was mirror polished with 1 μm, 0.3 μm and 0.05 μm alumina slurry and cleaned by sonication in (i) isopropanol, (ii) isopropanol: MilliQ water mixture and (iii) MilliQ water. Before alkanethiol adsorption the electrode was electrochemically cleaned by potential cycling between 0 and 1.6 V in 2 M H_2SO_4 at 10 $V.s^{-1}$, followed by a scan at 0.1 $V.s^{-1}$ to ensure surface cleanliness. The electrochemically active area was estimated from the gold oxide reduction peak.[19]

For ECSTM measurements evaporated Au films on glass with (111) preferred orientation (Gold arrandees™, Werther, Germany) were used as substrates. After soft annealing for 5 min with a hydrogen flame these Au substrates exhibit atomically smooth (111) terraces separated by monatomic steps in height.

For cyclic voltammetry measurements gold wires (polycrystalline Au), cleaned with piranha solution and rinsed with MilliQ water, were used as working electrodes. Gold arrandees (Au(111)) were also used for electrochemical measurements.

In all cases, SAMs were prepared by immersing the gold substrates into a freshly prepared alkanethiol 100 μM ethanolic solution for 24 h at room temperature, in the absence of light. Final rinsing was done with ethanol before drying under N_2(g).

Electrochemical experiments

Cyclic voltammetry was performed with a potentiostat with digital data acquisition (TEQ, Argentina) in a conventional three-electrode glass cell, using a large area platinum foil as counter electrode and a Ag/AgCl (3 M KCl) reference electrode. Alkanethiol modified gold wires were used as working electrodes and a 0.1 M NaOH solution purged with nitrogen was the electrolyte.

In some cases voltammetry was performed in the ECSTM cell using Au(111) as working electrodes and a Pd/H_2 reference electrode (see ECSTM experiments section). However, all potentials are reported with respect to a Ag/AgCl (3 M KCl) reference electrode.

Thiol reductive electrodesorption from both Au(111) and polycrystalline gold substrates was performed by scanning the potential from −0.2 to −1.7 V at 0.05 Vs^{-1} in 0.1 M NaOH electrolyte. In the case of Au(111) substrates the charge density involved in the alkanethiol reductive desorption process was ≈75 μC cm^{-2} (corresponding to a 0.33 coverage).

STM experiments

In air STM experiments were performed in the constant current mode with an ECM microscope and a Nanoscope IIIa controller from Veeco Instruments (Santa Barbara, CA). Mechanically cut Pt-Ir tips were used and typical bias voltages (E_{bias}), setpoint currents and scan rates were 0.5–1.2 V, 0.5–1 nA and 1–4 Hz, respectively.

ECSTM imaging was done in the constant current mode with the equipment described above and a bipotentiostat from Veeco Instruments (Santa Barbara, CA). Measurements were made in a small volume Kel-F electrochemical cell (ECSTM cell) using a high area Pt wire as counter electrode and a Pd/H_2 reference electrode. Deaerated 0.1 M NaOH solutions were used as electrolyte. Commercial Pt- Ir tips covered with nail polish were used. Typical tunneling currents and scan rates were 0.5– 3 nA and 1– 5 Hz, respectively. Working electrode (E_s) and tip (E_t) potentials were measured with respect to the Pd/H_2 reference, but in the text are reported referred to the Ag/AgCl (3 M KCl) electrode. E_t values were chosen so as not to have faradaic processes on the tip. All measurements were done at constant bias potential ($E_{bias} = E_t - E_s$).

Infrared experiments

PMIRRAS experiments were performed on a Thermo Nicolet 8700 (Nicolet, Madison, WI) spectrometer equipped with a custom made external tabletop optical mount, a MCT-A detector (Nicolet), a photoelastic modulator (PEM) (PM-90 with a II/Zs50 ZnSe 50 kHz optical head, Hinds Instruments, Hillsboro, OR), and a Synchronous Sampling Demodulator (GWC Instruments, Madison, WI).

A custom made Teflon® electrochemical cell was coupled to the set-up to acquire *in situ* IR spectra. The cell was connected to a Jaissle IMP88 Potentiostat (Germany) controlled by a homemade PMIRRAS acquisition software via a digital to analog converter (Agilent USB AD/DA converter). The IR window was a 1 inch (~25 mm) CaF_2 equilateral prism (Harrick Scientific Technology, PleasantVille, NY). Prior to the assembly of the spectroelectrochemical cell, the gold electrode was modified with the alkanethiol as detailed (see before). The cell was filled with a 0.1 M NaOH solution using deuterated water as solvent. All potentials were measured and reported with respect to a Ag/AgCl (3 M KCl) reference electrode.

The IR spectra were acquired with the PEM set for a half wave retardation at 2900 cm^{-1}. For spectra of the modified gold electrode in air, the angle of incidence was set at 80°, which gives the maximum of mean square electric field strength for the air/gold interface. The signal was corrected by the PEM response using a method described by Frey *et al.*[20] Typically 1500 scans were performed and the resolution was set for 4 cm^{-1}. In the case of spectroelectrochemical experiments the angle of incidence was set to 57°, which gives the maximum of mean squared electric field strength at the metal surface for the CaF_2/D_2O/gold cell. The thickness of the thin layer of electrolyte between the optical window and the gold electrode was typically set to 2.5 μm and was determined by comparing the experimental reflectivity spectrum of the thin layer cell attenuated by the layer of the solvent, to the reflectivity curve calculated from the optical constants of the cell constituents.[21,22] The demodulation technique developed in Corn's laboratory was used in this work. The absorbance of surface confined species in PMIRRA spectra is given by

$$\Delta S(\upsilon)=\frac{2\left|I_s - I_p\right|}{\left(I_s+I_p\right)}$$

where I_s and I_p are the intensities of s- and p-polarized light arriving to the detector.

A modified version of a method described by Buffeteau *et al.*[23] was used to correct the spectra for the PEM response. These corrections were performed using PEM functions measured for identical conditions to those used for spectral acquisition.[22] Finally, when *in situ* experiments are performed in a thin layer cell that contains electrolyte, the measured spectrum has a background due to absorption of the IR beam by the aqueous solution in the thin layer. To correct the spectra for the background, a baseline was built for each spectrum using the spline interpolation technique.

Five potential loops were performed in each experiment, varying the potential between −0.2 V and −1.7 V. Each potential step comprises an equilibration time of 3 minutes followed by the acquisition of the spectrum by averaging of 1500 scans at 4 cm^{-1} resolution, which typically takes 25 minutes.

Determination of molecular orientation of the SAMs

The molecular orientation of the chains was determined using the “relative” method approach,[24–26] which relies on the availability of at least two absorption modes that correspond to differently oriented dipoles. It is based on the so called ‘surface selection rules’ that state that when linearly polarized light is absorbed by a sample, the integrated intensity of the absorption band is proportional to the square of the absolute value of the dot product of the transition dipole vector and the electric field vector of the incident radiation[21]:

$$\int A d\nu \propto \Gamma\left|\vec{\mu}\cdot\vec{E}\right|^2=\Gamma|\mu|^2|E|^2\cos^2\Theta$$

At the metal surface, the direction of the electric field vector of the p-polarized radiation is normal to the surface. Therefore the integrated band intensity of adsorbed molecules is proportional to $\cos^2\Theta$, where Θ is the angle between the average direction of the transition dipole moment and the normal to the surface.[21]

In this case the CH_2 and CH_3 absorption bands were used. Briefly, in the alkanethiol SAMs the CH_3 has a relatively free rotation and is quite mobile, so it can be assumed to have no preferential orientation, i.e. $\cos^2\Theta_{CH3}=1/3$, while CH_2 dipoles are related to the chain orientation. In a transmission experiment, the alkanethiol orientation is randomly distributed in the KBr pellet, so both CH_2 and CH_3 are randomly distributed. Relative differences in the IR peak areas for CH_2 and CH_3 stretching modes between the alkanethiol SAM and the randomly distributed solutions can be attributed to a preferred orientation for the alkane chain in the SAMs. The relationship between the areas of these peaks can be written as:

$$\frac{A^R_{CH2}}{A^R_{CH3}}=\frac{A^T_{CH2}}{A^T_{CH3}}\cdot\frac{\cos^2\Theta^R_{CH2}}{1/3} \quad (1)$$

Where A^R is the peak area of a mode in the SAM, A^T is the peak area in a randomly distributed sample, and Θ^R_{CH2} is the angle between the CH_2 transition dipoles and the surface

normal. The main contribution to errors involved in this method arises from the maximum absorbance determination. In this case the Relative Standard Deviations (RSD_{RAS}) is assumed to be 5%.[26]

The spectra were fitted by 5 gaussians. $\nu_a(CH_3)$ and $\nu_s(CH_2)$, being the more isolated peaks, were chosen to calculate the angles.

MD Simulations

In this work, both the adsorbed state and the electrodesorption process of alkanethiol SAM on gold substrate have also been studied by MD simulations. The simulated system consists of 126 alkanethiol molecules (either C12 or C18 chains), in water with 0.1M NaCl as an electrolyte, on a monoatomic layer of Au(111) containing 378 Au atoms. The alkanethiol molecules were described by the united-atom model developed by Hautman and Klein.[27] The parameters of the Lennard-Jones potentials involving Au atoms were taken from Zhao *et al.*[28]. In the simulations, the positions of the gold atoms have been constrained to remain fixed. While the dynamics of Au atoms is expected and may play a role in the electrodesorption process of alkanethiols, our focus in this study is on the behavior of the desorbed alkanethiol chains, and the treatment of the Au atom mobility is beyond the scope of this work. Water molecules were described using the TIP4P model. The number of water molecules in the simulation boxes ranged around 7100 for the C12 chain systems and around 6600 for the C18 chain systems.

The chemically adsorbed alkanethiols on Au substrate were modeled by assigning a Morse potential for Au-S bond while assigning a zero formal charge on Au and S atoms. The parameters of the Morse potential have also been obtained from Zhao *et al.* [28]. The nearest Au-Au distance in Au(111) substrate in the simulation is set at 2.884 Å, and the alkanethiol chains were initially placed at three-way hollow sites, $2.884 \times \sqrt{3} = 5.0$ Å apart, so that the sulfur head groups form a $\sqrt{3}\times\sqrt{3}$ R30° lattice. The equilibrium Au-S bond length is 2.65 Å.

The electrodesorption process of alkanethiols has been modeled by removing the explicit Au-S bonds (i.e., turning off the Morse potential) and assigning negative formal charges on Au and S atoms. As the formal negative charges were added to the Au and S atoms, extra Na^+ ions were included in the system in order to maintain the overall charge neutrality. More details on the modeling of the electrodesorption in our simulations are presented in the Results and Discussion section.

Periodic boundary condition was implemented at all box boundaries. The dimensions of the simulation box are $6.0564 \times 4.49571 \times 20$ nm^3, including a 10.0-nm thick vacuum layer on top of the SAM-water system, which was added in order to avoid the interaction of periodic images in z-direction. The geometric combination rules have been employed for cross interactions between hetero-atoms. The long-range electrostatic interactions were calculated via Particle-Mesh Ewald (PME) algorithm. All simulations were run at room temperature of 298 K. In a typical MD simulation, the system is first energetically stabilized by the steepest descent algorithm, followed by a production run for 10 ns at room temperature of 298K. The MD simulations were run using the GROMACS simulation package, version 4.5.4.[29]

Results and Discussion

Electrodesorption of dodecanethiol and octadecanethiol SAMs on Au

Figure 1 shows current-potential curves recorded in a conventional 3-electrode glass cell corresponding to C12 (a) and C18 (b) SAMs on Au(111) electrode, both at 0.050 Vs^{-1} in 0.1 M NaOH electrolyte. For C12, a reductive desorption peak preceding the hydrogen evolution reaction (HER) can be observed at -1.12 ± 0.03 V, while for C18 on Au(111) the

desorption peak appears at −1.22 ± 0.05 V (vs Ag/AgCl (3 M KCl)). For polycrystalline Au the C12 desorption peak appears at −1.35 ± 0.03 V, while for C18 it is a poorly defined hump located at ~ −1.5 V, which overlaps with the HER current (data not shown). Reductive desorption from these surfaces has been previously described for similar alkanethiols.[30,31] This peak has been attributed to reaction:[12]

$$Au{-}S(CH_2)_nCH_3{+}e^- \rightarrow Au^0{+}{}^-S(CH_2)_nCH_3 \quad [1]$$

After reversing the potential scan, a smaller peak at more positive potentials corresponding to the readsorption of the desorbed thiolates is observed for both substrates. The small difference between the cathodic peak (desorption) and anodic peak (readsorption) charge densities has been assigned to the loss of desorbed thiolates by diffusion to the bulk solution. The charge density of the cathodic peak is ≈75 μC cm^{-2}, consistent with the desorption of the dense standing-up √3×√3 R30° and c(4×2) lattices, both with surface coverage θ = 0.33. Even though a reasonable estimation of the SAM surface coverage can be obtained by this technique, one should be aware that it could involve a 10% error with respect to the SAM coverage obtained by other techniques, like X-ray Photoelectron Spectroscopy (XPS) (data not shown).[32–35]

In-air STM imaging of alkanethiolate-modified Au(111) before and after desorption

Figure 2 shows typical in-air STM images of a C12 SAM on Au(111) (a, b) before and (c) after complete desorption. The dark features in Figure 2a correspond to gold vacancy islands (“pits”), usually of the height of a gold atom, and nowadays considered a consequence of the Au atom removal from terraces to form the thiolate-gold adatom species. As mentioned in the Introduction, several models have been proposed from DFT calculations for both the √3×√3 R30° lattice and especially for the c(4×2) superlattice.[1,4,5,7] Among the latter models, the most widely accepted for the c(4×2) lattice involves $(RS)_2$-Au complexes,[5] and therefore requires a 0.165 Au adatom coverage (1 adatom every 2 alkanethiol molecules). For C12 SAMs, the most commonly found lattice is by far the √3×√3 R30° (see high resolution image in Figure 2b), although, as already discussed elsewhere,[36] some c(4×2) domains can be also found on the Au surface. In terms of adatom models the √3×√3 R30° lattice could be explained by the presence of RS-Au species, as proposed by Woodruff et al.[4] However, in contrast to the models containing $(RS)_2$-Au species, the thermodynamic stability of the model proposed in reference 4 is lower that the unreconstructed Au surface since it needs a larger amount of Au adatoms (0.33, i.e. 1 adatom every 1 alkanethiol molecules).

From the analysis of many STM images of large, flat Au(111) terraces covered by C12 SAMs (far from step edges) a θ_{pits} value ~0.14 is obtained (lower part of Figure 2b), a figure that would be in good agreement with the existence of $(RS)_2$-Au moieties (although present $(RS)_2$-Au models are not strictly applicable to the √3×√3 R30° lattice). As in the case of other alkanethiols, the small difference could be accounted for by the contribution of some amounts of Au adatoms from the lifting of the 22×√3 surface reconstruction. Note that θ_{pits} ~0.14 is markedly larger than that recently reported for butanethiolate SAMs on Au(111).[6]

Following complete desorption, and based on the above mentioned adatom models, we would expect the formation of Au islands of monoatomic height. This is indeed the case, as it is shown in Figure 2c and the cross section of the islands (Figure 2d). In this case a C12 SAM on Au(111) has been thoroughly electrodesorbed in a 0.1 M NaOH solution, removed from the cell, rinsed and dried, and then imaged by in air STM. The absence of thiol molecules on the surface has been checked by XPS (data not shown). Islands ~0.24 nm high (consistent with Au monoatomic height islands) can be observed, with θ_{isl}~ 0.07. This coverage - smaller than expected for desorption of the √3×√3 R30° lattice and c(4×2)

superlattice containing RS-Au (θ_{isl}~0.33) or $(RS)_2$-Au moieties (θ_{isl}~0.165) – can be explained by the fact that the Au adatoms produced by reaction [1] partially fill the gold vacancy islands.

In fact, θ_{pits} is now reduced from 0.14 (before desorption) to 0.07 (after desorption). Interestingly, our results contrast with $\theta_{isl} \approx 0.22$ for thiol desorption induced by water electrolysis assisted by STM tips.[17] Therefore, the analysis of the structures formed during *in situ* thiol desorption, i.e. in contact with the electrolyte solution, deserves special attention.

In situ electrodesorption of dodecanethiol SAMs on Au

The electrochemical desorption of dodecanethiol was studied both by ECSTM and PMIRRAS. Figures 3a–d show sequential ECSTM images of the same region of a C12 SAM on Au(111) taken in 0.1 M NaOH under electrochemical control. In Figure 3a (E_s = −0.69 V, i.e., at a potential more positive than that of the reductive desorption peak) pits can be clearly observed with θ_{pits} ~0.14, as found in the *ex-situ* images. However, when the applied potential is shifted to −0.93 V (at the onset of the desorption peak), some bright spots (Fig 3b–d) 0.7 ± 0.1 nm in height appear on the surface (see also Fig. 4d). The comparison of Figures 3b–d shows that the spot density increases as a function of time ((b) t= 0; (c) t= 3 min, (d) t= 6 min). At even longer times the surface is almost completely covered by the bright spots, which are swept away by the tip (data not shown). As already reported,[8] some pit coalescence can be observed as a function of time (see squares in Figs. 3a and 3b). ECSTM images of a C12 SAM on Au(111) corresponding to another sample are shown at −0.69 V (Fig 4a) and −1.00 V (Fig 4b). In this case, since the electrode potential was shifted more negatively than that in the images in Figure 3 (−0.93 V), although still at values corresponding to the onset of desorption (i.e. more positive than the desorption potential), a higher density of bright features on the terraces is found.

Similar bright spots have been previously reported from ECSTM electrodesorption experiments of other alkanethiol SAMs[10,15,16] in alkaline media and have been attributed to micelles, or some kind of aggregates, of physisorbed alkanethiols. In Figure 4c, a higher magnification image of the same sample as in Figure 4b shows that the bright spots (see green arrows), which are 0.7 ± 0.1 nm in height (see histogram in Fig. 4d), coexist with an underlying pattern of aligned rows with distances 3.9 ± 0.2 nm (see dotted rectangles in Fig 4b), a value that is close to twice the dodecanethiol length (~1.9 nm).[37] This would indicate that the rows correspond to a lying down phase of thiol molecules in a S-head to S-head configuration.[3] Note that the bright spots are aligned perpendicular to the rows of lying down molecules.

It is clear that the features shown in Figures 3 and 4 cannot be assigned to simple Au islands, as suggested in other works, [8,17,18] since they should be 0.24 nm high (see cross section in Figure 2d) and have sharper edges. Also, in some cases, it is possible to resolve a fine molecular structure inside them, as shown in Figure 4e. These results support the idea that the bright spots observed during in situ imaging are formed by desorbed alkanethiolates that remain near the Au surface. Some of these alkanethiolates can be oxidatively readsorbed if the potential scan is reversed (see Figure 1).

PMIRRAS of C12 and C18 SAMs on gold in air and under water

PMIRRAS was used to characterize typical C12 and C18 SAMs on Au in air and in contact with an electrolyte solution, *i.e.* under open circuit conditions. Figure 5 shows typical spectra in the CH stretching region (3000–2800 cm^{-1}) both in air and in 0.1 M NaOH in D_2O solution. Similar spectra and band assignment have been reported[11,18,19,38,39] and are

used here to compare with our spectra. Briefly, the band at ~2960 cm^{-1} is assigned to the CH_3 asymmetric stretching mode ($\nu_a(CH_3)$), while the band at ~2875 cm^{-1} is assigned to the CH_3 symmetric modes ($\nu_s(CH_3)$). The bands at ~2920 and ~2850 cm^{-1} are assigned to ν_a and ν_s CH_2 modes, respectively, while that at ~2935 cm^{-1} is assigned to a Fermi resonance (FR) which is the combinational band of the CH_2 symmetric stretching vibration at 2850 cm^{-1} and the second harmonic of CH_2 bending vibration at 1467 cm^{-1}. As expected for a long chain alkanethiol, the peak position of the methylene asymmetric stretching, $\nu_a(CH_2)$, corresponds to well-ordered, pseudo-crystalline monolayers[40] (2919 and 2918 cm^{-1} in air for C12 and C18 respectively). Upon D_2O immersion, a small change in the position of the stretching peaks occurs, especially for C12, probably because of the intercalation of some solvent molecules among the alkyl chains.[15]

In situ PMIRRAS of C12 and C18 SAMs on gold under electrochemical control

In situ PMIRRA spectra were acquired at selected applied potentials going from the region where the SAM is expected to be stable (starting at −0.2 V) to the potential region where alkanethiol desorption has already taken place (−1.7 V) and then back to −0.5 V (see Figure 1). Four loops were performed. In the first loop, in order to have a close look at the desorption process, measurements were made in 0.025 V steps, from −0.8V to −1.2V (before, at the onset of, and after the electroreduction process). The subsequent spectra were taken at 0.25 V steps in order to study the response of the system to potential cycling. Figure 6 shows the peak area of $\nu_a(CH_3)$ and $\nu_a(CH_2)$, the position of the maximum of the $\nu_a(CH_2)$ peak, and the calculated angle of the dipole moment of the $\nu_s(CH_2)$ with respect to the surface normal (Θ) as a function of the applied potential for the four consecutive desorption loops. PMIRRAS experiments are based on the 'selection rules' of the surface and thus the technique is sensitive to IR absorbing species that are either adsorbed on, or at distances smaller than a few microns from the surface.[21] First, we will analyze the behavior of the $\nu_a(CH_3)$ signal (Figure 6 top). Since CH_3 has no preferential orientation, the areas of both $\nu_a(CH_3)$ and $\nu_s(CH_3)$ are indicative of the amount of alkanethiol adsorbed on the surface (or close to it). From the analysis of the $\nu_a(CH_3)$ intensity in Figure 6 it can be seen that only a small fraction of the initial alkanethiol molecules leave the Au surface after the completion of the first loop. Complete desorption for C12 involves at least four loops. Therefore, the IR results confirm that the bright spots shown in the in situ STM images (Figure 3–4) taken in the first negative excursion contain significant amounts of alkanethiolates and cannot be considered as simple Au islands.

The behavior of the $\nu_a(CH_2)$ peak gives detailed information about the chain ordering during desorption. The dipole moments of CH_2 symmetric and asymmetric stretching modes are perpendicular to the alkanethiol backbone. As a result, the area of the absorption band of $\nu_a(CH_2)$ and $\nu_s(CH_2)$ increases when the angle between the alkyl chain and the normal to the surface increases.

Figure 6 shows that the peak area of $\nu_a(CH_2)$ markedly increases at potentials corresponding to the onset of the desorption peak (in figure 6, the zones marked in cyan correspond to the applied potentials between the onset of desorption (~−1.05 V) and the beginning of readsorption (~−0.95 V) of thiols according to cyclic voltagrams in figure 1 This behavior can be interpreted as a result of an increase in the angle between the normal to the surface and the alkanethiol backbone. It should be noted that, if the alkyl chains were completely desorbed and randomly distributed, the calculated angle Θ would be 54.7°.[21] The fact that upon desorption potentials the angle Θ decreases to almost 45° (Figure 6) means that the weighted average tilt angle of the chains ($<\alpha>$) would be around 45° (the dipole moment of both the symmetric and asymmetric stretchings of CH_2 are perpendicular to the hydrocarbon backbone).[21] This condition could be achieved with most of the alkyl chains at ~45° or with some lying down and the rest randomly distributed or at some preferential angle. This last

assumption is in agreement with ECSTM experiments, where the onset of desorption seems to involve the formation of domains of lying down molecules with 3.9 ± 0.2 nm separation (Fig. 4b and c) that coexist with the bright spots formed by thiol molecules in aggregates with random orientation. After the initial rise, the area of the $\nu_a(CH_2)$ peak decreases markedly, suggesting that the thiol molecules that remained chemisorbed in a lying down configuration are desorbed and randomly distributed at small distances from the electrode (therefore visible by PMIRRAS, with Θ close to 54.7°), either forming new aggregates or incorporating into existing aggregates. When the potential scan is reversed towards more positive potentials, and readsorption potential is reached, the peak area of the $\nu_a(CH_2)$ starts to increase to reach, at the end of the first loop (at −0.5 V), a value similar to that measured before the desorption run. This behavior correlates with the oxidative readsorption process shown in the voltammograms (Figure 1). Moreover, the maximum of the peak diminishes from 2921 cm^{-1} to 2919 cm^{-1}, a quasi-crystalline value, i.e. the SAMs become slightly more ordered after the first loop (see Figure 6). This result is in agreement with what was observed by Anderson *et al.* for octadecanethiol SAMs on gold in acetonitrile when reductive potentials were applied.[16] In the following loops, the position of this peak moves to higher values (from 2919 to 2921 or 2923 cm^{-1}) when desorption potential is applied (−1.7 V, the cyan zones in figure 6), and goes back to the lower value when the potential is reversed, indicating that the alkyl chains curl or get more disordered upon desorption and readsorb in an ordered, quasi-crystalline fashion. The behavior of the $\nu_a(CH_2)$ signal during the first loop is repeated in the consecutive cycles, although the area of the peak decreases continuously following the same trend observed for the area of the $\nu_a(CH_3)$, showing that there is a continuous desorption and loss of molecules from the Au(111) surface, in agreement with the electrochemical data in Figure 1. Therefore, from the STM and PMIRRAS results we conclude that when the C12 SAM desorption takes place, such process leads to the formation of disordered micellar alkanethiolate aggregates. This structure contrasts to that presented in Ref.[11] for C16 SAM desorption, where micelles consisting of thiolates placed parallel to the Au surface were proposed from in situ AFM force curve measurements. Therefore, we decided to analyze the desorption of a longer thiol (C18) to evaluate the influence of the chain length on the alkanethiolate structures. In this case ECSTM was not performed because very low currents[41] (hardly achievable under electrochemical control) are needed for such long alkyl chains. Thus, an average picture was obtained from PMIRRAS measurements.

These results are shown in Figure 7. In the first loop we note, from the area of the $\nu_a(CH_3)$ peak, that almost 100% of the thiolates remain at the interface, as observed for C12 SAM desorption (Figure 7, top panel). The same trend as for C12 is also observed along the successive loops: there is a slow but progressive loss of thiolates towards the electrolyte solution. However, in contrast to what was observed for C12, the position of the IR absorbing peaks does not change appreciably upon potential application, as neither $\nu_a(CH_2)$ nor $\nu_s(CH_2)$ change from their “crystal-like” values (2918 cm^{-1} and 2850 cm^{-1}, respectively, data not shown). This fact indicates that the hydrocarbon chains remain fully extended and close packed during the whole potential cycle, even during desorption-readsorption process. On the other hand, the area of the $\nu_a(CH_2)$ peak decreases when reaching desorption potentials (from ~−1.15 V in the cathodic sweep to ~−1.05 V in the anodic sweep, the cyan zones in figure 7) and recovers, though not to the initial point, when the applied potential returns to oxidative values and readsorption occurs. This means that, upon desorption, the average angle between the hydrocarbon chains and the normal to the surface (<α>) diminishes from the ~30° value determined by the directionality of the the Au-S-CH_2 bond.[42,43] PMIRRAS results also suggest that when desorption starts the monolayer desorbs as a whole, since the positions of the symmetric and antisymmetric CH_2 stretching peaks do not change in the overall process

At still more reductive potentials, as desorption is complete, the alkyl thiols seem to remain close to the electrode, and as a result they are still visible by PMIRRAS. When the potential is reversed, the thiols are readsorbed on the surface, and the 30° angle is recovered due to the covalent character of the Au-S bond, and accordingly the area of the CH_2 stretching peaks increases again.

Summarizing, from PMIRRAS experiments we can conclude that the behavior of the different length thiols is different upon reductive desorption. In the case of C12, at the onset of desorption, based on the increase of the tilt angle, and combined with STM experiments, we propose that some molecules desorb forming micelles, while others lie flat on the surface. As the reduction potential is reached, all the molecules desorb, most of them staying close to the electrode, curled, in a randomly oriented way, probably forming micelles, as indicated by the increase of the position of the maximum of the $\nu_a(CH_2)$ peak and the experimental 54.7° tilt angle. As the potential is reversed, most of the thiol molecules readsorb on the surface in an ordered way, somehow recovering the initial structure. On the other hand, the electroreduction of C18 proceeds as a whole. The thiols stay ordered and elongated during the whole process as indicated by the constant value of 2918 cm^{-1} for the maximum of $\nu_a(CH_2)$ peak during the whole experiment. The average angle of the alkyl chains decrease at desorption potentials, indicating that the directionality of the Au-S bond is lost. As the potential is reversed the thiols readsorb recovering the initial structure.

These results suggest that the desorption processes for C18 and C12 are quite different. In order to clarify this point, we carried out MD simulations of the desorption of C12 and C18 SAMs.

MD simulations of C12 and C18 SAMs on Au in vacuum and in water

MD simulations have been performed in vacuum for a C12 SAM on a Au(111) substrate and the final snapshot is shown in Figure 8a. Note that, in order to simplify our simulations, we have considered all alkanethiolate SAMs on unreconstructed Au(111) surfaces, i. e., no Au adatom species are present, taking into account that we are interested in explaining the structural changes in the alkanethiol aggregates inferred from PMIRRAS data.

The alkanethiol molecules are aligned in the well-known √3×√3 R30° lattice structure with the average chain-chain distance of ~5.0 Å. The α angle of the C12 alkanethiol molecules in the final 1ns of the simulation shows a narrow Gaussian distribution with the maximum near 28° (Figure 8b). Upon the immersion of the C12 SAM in water, the tilt angle distribution changed slightly, with the overall distribution shifting to larger angles by ~2°. In the case of the C18 alkanethiol SAM, on the other hand, the tilt angles show similar average values around 32° in both vacuum and water, with significantly smaller fluctuations in water (Figure 8b). The alkanethiol SAMs in our simulations for the adsorbed cases form a well-ordered quasi crystalline phase with little or no defects, thus the intercalation of water among alkyl chains, as suggested from the PMIRRAS spectral change for the C12 SAM with a less-ordered structure and defects (like the disordered regions at domain boundaries and pits observed by STM), was not observed in the simulations.

The electrodesorption process of the alkanethiol SAM from the Au(111) substrate has been modelled by implementing several changes to the adsorption model. 1) We eliminated the Au-S bond defined by the Morse potential. This assumes that all S-Au bonds break completely and instantaneously when the reductive desorption of alkanethiol from Au substrate is initiated by the electrode potential. 2) We added a formal charge of $-1.0\ e^-$ on the sulfur atom of each alkanethiol chain in order to match the formal charge of the thiolate molecule, the product species of the electrodesorption reaction [1]. 3) Finally, a negative formal charge, q_{Au}, was assigned on each Au atom in order to reflect the fact that the surface

charge is negative at the desorption potential. As the negative formal charges are added to the S and Au atoms, we have added extra Na^+ ions to the bulk water to maintain the charge neutrality of the system. Since the information on the experimental surface charge of the Au(111) substrate is not available for the given applied potentials, we arbitrarily chose three different surface charges, $q_{Au} = -0.05$, −0.2, and −0.4 e^-, in order to monitor the system behavior against different surface density of charge. The number of extra Na^+ ions added to compensate for the negative charges of the Au and S atoms was 145, 202, and 277 for $q_{Au} = -0.05$, −0.2, and −0.4 e^-, respectively.

Figure 9a shows the final snapshots of the C12 SAM for the three different charges on the surface Au atoms. In all three cases, around 50% of all molecules remain near the surface with their sulfur atoms close to their original positions, paired with Na^+ ions to neutralize the S-S and S-Au electrostatic repulsions. Around 30% of all alkanethiol chains also remain near the surface, either disordered or upside down, with their sulfur atoms mostly interfacing with the water phase. This results in the formation of a structure similar to a bilayer, with some of the stretched alkanethiol molecules in the upper and lower leaflet interdigitating to each other in the cases of the surface charge of $q_{Au} = -0.05$ and −0.2 e^-, as shown in Figure 9a. As the surface charge becomes more negative ($q_{Au} = -0.4$ e^-), the bilayer-like structure disappears and the alkanethiol molecules near the surface become more disordered with an increase in the lying-down phase, as observed in the experiments. The lying-down phase of the C12 alkanethiol molecules is shown explicitly in the lower right side of the figure. The type of structures that are formed seem more reminiscent of micelle-like structures. A small fraction of the alkanethiol molecules, typically 10–20% of all chains, immediately leaves the surface into the bulk water at the very early stage of the simulations and remains in the bulk throughout the simulations, in agreement with the diffusional loss of the C12 chains observed in the electrodesorption experiments. near the Au(111) surface are shown in Figure 9b. The distributions confirm the bilayer-like structure with peaks at $\alpha \approx 15°$ (almost upright stance) and ≈170° (near upside-down stance) for $q_{Au} = -0.05$ and −0.2 e^-, and the formation of lying-down phase with tilt angles near 80° in combination with the more disordered structure for $q_{Au} = -0.4$ e^-. This suggests that the simulation with $q_{Au} = -0.4$ e^- matches well with the experimental observation in the case of the C12 SAM desorption. The comparison between the experiments and the simulations can also be made for the average tilt angle $\langle\alpha\rangle$, which was estimated to be around 45° upon the reductive desorption of C12 alkanethiol molecules according to the PMIRRAS data. Note that PMIRRAS measures the squared quantity of the surface normal component of the CH stretching modes, so the alkanethiol molecules with tilt angle α and $(180° - \alpha)$ register the same spectral intensity. Therefore, for proper comparison with the experiments, the average tilt angle $\langle\alpha\rangle$ was calculated for the simulations after first converting the tilt angles α greater than 90° to $(180° - \alpha)$ from Figure 9b. The results are shown in the inset of Figure 9b, where the case with $q_{Au} = -0.4$ e^- again agrees very well with the experimental value of 45°.

The results from the simulations reveal the important role of the Na^+ counterion in stabilizing the desorbed alkanethiolate molecules near the surface. The simulations also show the formation of the lying-down phase in the complete absence of the S-Au covalent bonds, suggesting that the lying-down phase of the alkanethiol molecules does not necessarily require the presence of the S-Au covalent bonds, and that the ion-pair formation with Na^+ is enough to stabilize the thiolate species and to retain them near the negatively charged electrode surface. On the other hand, the role of Cl^- ions in our simulations is that of a simple electrolyte introduced to reproduce the conditions of the electrodesorption experiments. Since the surface and the thiolates are both negatively charged, Na^+ ions play crucial role in stabilizing the thiolate species, while Cl^- ions mostly stay in the bulk water phase (sufficiently far from the surface) in our simulations and do not play a significant role in the electrodesorption process of alkanethiols.

Figure 10a shows the final snapshots of the C18 SAM from 10-ns MD simulations for the electrodesorption process with the formal charge on the surface Au atoms at $q_{Au} = -0.05$ (top), −0.2 (middle), and −0.4 e^- (bottom). Similar to the simulation results of the electrodesorption for C12 SAM, the desorbed C18 alkanethiols form a bilayer structure with the stretched alkanethiol chains at the upper and lower leaflet interdigitating to each other. The interdigitation of the C18 alkanethiol chains in the bilayer appears to be more complete than for the C12 case, especially at the surface charge $q_{Au} = -0.05$ and −0.2 e^-. Compared to the C12 SAM aggregates shown in Figure 9a, at the surface charge $q_{Au} = -0.4$ e^- the bilayer structure formed by the desorbed C18 molecules remains relatively robust in the mix, though with increasingly disordered chain orientations. The tilt angle distributions of the desorbed C18 alkanethiol chains in Figure 10b supports the enhanced structural definition of a bilayer for the desorbed alkanethiol aggregates, with the sharp peaks near $\alpha = 20°$ and 160° for the surface charge $q_{Au} = -0.05$ e^-, and the relatively narrow peaks near 30° and 150° for $q_{Au} = -0.2$ e^-. At $q_{Au} = -0.4$ e^- the peaks near $\alpha = 35°$ and 150°, in combination with a decrease in the lying down phase in the simulations relative to the case for the C12 aggregates, represent an enhanced structural robustness for the C18 aggregates over the given range of the surface charge. Again, Na^+ ions arrange among negatively charged sulfur atoms to stabilize the chain aggregation, playing a critical role in defining the behavior of the alkanethiolate

The bilayer formation with a well-ordered, compact quasi crystalline structure and a decrease in the tilt angle for the desorbed C18 aggregates at $q_{Au} = -0.05$ e^- in the simulation matches well with the experimental observations. The simulation confirms that the overall chain-chain distance between the alkanethiol molecules decreases upon the rupture of the Au-S covalent bonds, as conjectured above, resulting in the decrease in the tilt angle. On the other hand, the simulation shows that a small fraction of the alkanethiol molecules escape to the bulk water during the desorption process, in accordance with the slow and progressive diminution of $\nu_a(CH_3)$ observed in PMIRRAS experiments for C18 SAMs. It is also notable that the best match of the simulation with the experimental observations is found at the weakest surface charge considered ($q_{Au} = -0.05$ e^-) in the C18 case, whereas the best agreement with the experiments for the C12 case was identified at the strongest surface charge ($q_{Au} = -0.4$ e^-). These results could be explained considering that the potential of zero charge (PZC) is very similar for both C12 and C18 on Au(111) (−0.51 V and −0.53 V, respectively) [44], but the two SAMs have different double layer capacitances, larger for C12 than for C18 due to the higher number of defects, pinholes, etc. for shorter chain lengths (1.8 and 0.8 μF cm^{-2} for C12 and C18, respectively).[44] Therefore, for a given applied potential, more ions and water molecules can penetrate the C12 SAM compared to the C18 SAM, and accordingly this results in a larger negative charge on the metal,[45] favoring thiol electrodesorption. Thus, although the chosen q_{Au} values are arbitrary, we emphasize that the electrodesorption of the two studied alkanethiols is qualitatively different.

In this work, the MD simulations of the desorption process only attempt to model the thiolate species that are already completely desorbed. Both processes, the Au-S bond breaking that occurs during the cathodic potential scan and the bond formation that occurs during the anodic scan are not explicitly considered. More complete translation of the structural outcomes of the MD simulations into the conductivity patterns of the ECSTM would require quantum mechanical computations that properly incorporate the Au-S bond breaking and reformation processes during the potential loop, which is computationally extremely expensive and beyond the scope of this work.

Concluding remarks

The desorption-readsorption process of C12 and C18 was studied. The C12 behavior was characterized in more detail, combining ECSTM, PMIRRAS under electrochemical control and MD simulations. The analysis of pit coverage before desorption seems to be consistent with the presence of RS_2Au species, a fact that will require further investigations in terms of the new adatom models. Upon arrival to the potential where the onset of desorption starts, a partial alkanethiol desorption occurs, resulting in the formation of domains of a lying-down alkanethiol lattice that coexists with aggregates of physisorbed alkanethiolates in a random configuration. Shifting the potential towards the desorption peak accelerates thiol desorption, and molecules remain close to the electrode in a random distribution, forming larger aggregates. It is important to stress that the observed features are not simple Au islands and that these can only be obtained after a careful ex situ cleaning procedure. As the potential is reversed, part of the thiol molecules readsorb with a tilt angle of around 30° and form a more ordered SAM. The behavior of the system during the first potential loop is repeated in the consecutive cycles with continuous desorption and loss of molecules from the Au(111) surface.

As regards C18, its desorption behavior is different probably due to a higher interaction among alkyl chains. In this case, based on the lack of change of the positions of the maxima of the symmetric and asymmetric CH_2 stretching peaks, the SAM seems to maintain its order and a standing up configuration during the whole desorption-readsorption process. According to MD simulations, a bilayer structure is formed with alkanethiol chains at the upper and lower leaflet interdigitating to each other. Also, depending on the initial conditions, MD simulations show that the desorbed chains may remain near the surface, maintaining their well ordered quasi crystalline structure. When the potential is reversed most of the thiols readsorb on the surface at angles ~30°, as the directionality of Au-S-CH_2 bond prevails.

Our results show that the complexity of thiol electrodesorption in aqueous electrolytes is clearly much greater than the desorption processes that take place in vacuum, either induced by a temperature increase or by exposure to atomic hydrogen. They also open a question about the interpretation of tip-induced thiol desorption in moist air, including the crucial role of the chain length in the desorption- readsorption process.

Acknowledgments

This work has been supported by ANPCyT (PICT 06-621), CONICET (PIP112-200801-00362) and UNLP (11/X531) grants. E. P. gratefully acknowledges a doctoral fellowship from CONICET- ANPCyT. S.H.P. and I. S. thank the financial support from NIH grant R01 EB005772, and G.S.L thanks an NSF postdoctoral fellowship, NU-MRSEC DMR-0520513 at Northwestern University.

References

1. Vericat C, Vela ME, Benitez G, Carro P, Salvarezza RC. Chemical Society Reviews. 2010; 39:1805. [PubMed: 20419220]
2. Pensa E, Cortés E, Corthey G, Carro P, Vericat C, Fonticelli MH, Benítez G, Rubert AA, Salvarezza RC. Accounts of Chemical Research. 2012
3. Vericat C, Vela ME, Salvarezza RC. Physical Chemistry Chemical Physics. 2005; 7:3258. [PubMed: 16240039]
4. Yu M, Bovet N, Satterley CJ, Bengió S, Lovelock KRJ, Milligan PK, Jones RG, Woodruff DP, Dhanak V. Physical Review Letters. 2006; 97:166102. [PubMed: 17155415]
5. Grönbeck H, Häkkinen H, Whetten RL. The Journal of Physical Chemistry C. 2008; 112:15940.

6. Wang Y, Chi Q, Hush NS, Reimers JR, Zhang J, Ulstrup J. The Journal of Physical Chemistry C. 2011; 115:10630.
7. Maksymovych P, Voznyy O, Dougherty DB, Sorescu DC, Yates JT Jr. Progress in Surface Science. 2010; 85:206.
8. Arce FT, Vela ME, Salvarezza RC, Arvia AJ. Electrochimica Acta. 1998; 44:1053.
9. Taylor R, Torr N, Huang Z, Li F, Guo Q. Surface Science. 2010; 604:165.
10. Vericat C, Andreasen G, Vela ME, Martin H, Salvarezza RC. Journal of Chemical Physics. 2001; 115:6672.
11. Allara DL, Nuzzo RG. Langmuir. 1985; 1:52.
12. Walczak MM, Popenoe DD, Deinhammer RS, Lamp BD, Chung C, Porter MD. Langmuir. 1991; 7:2687.
13. Yang DF, Al-Maznai H, Morin M. The Journal of Physical Chemistry B. 1997; 101:1158.
14. Byloos M, Al-Maznai H, Morin M. The Journal of Physical Chemistry B. 1999; 103:6554.
15. Anderson MR, Evaniak MN, Zhang M. Langmuir. 1996; 12:2327.
16. Anderson MR, Gatin M. Langmuir. 1994; 10:1638.
17. Allara DL, Nuzzo RG. Langmuir. 1985; 1:45.
18. Allara DL, Swalen JD. The Journal of Physical Chemistry. 1982; 86:2700.
19. Finklea HO, Snider DA, Fedyk J. Langmuir. 1990; 6:371.
20. Frey, BL.; Corn, RM.; Weibel, SC., editors. Polarization-modulation Approaches to Reflection-Absorption Spectroscopy. Vol. Vol. 2. John Wiley & Sons; 2001.
21. Zamlynny, V.; Lipkowski, J. Advances in Electrochemical Science and Engineering. Alkire, RC.; Kolb, DM.; Lipkowski, J.; Ross, PN., editors. Vol. Vol. 9. Weinheim: WILEY; 2006.
22. Zamlynny V, Zawisza I, Lipkowski J. Langmuir. 2002; 19:132.
23. Buffeteau T, Desbat B, Blaudez D, Turlet JM. Applied Spectroscopy. 2000; 54:1646.
24. Arnold R, Terfort A, Wöll C. Langmuir. 2001; 17:4980.
25. Debe MK. Journal of Applied Physics. 1984; 55:3354.
26. Grumelli D, Méndez De Leo LP, Bonazzola C, Zamlynny V, Calvo EJ, Salvarezza RC. Langmuir. 2010; 26:8226. [PubMed: 20356031]
27. Hautman J, Klein ML. The Journal of Chemical Physics. 1989; 91:4994.
28. Zhao X, Leng Y, Cummings PT. Langmuir. 2006; 22:4116. [PubMed: 16618153]
29. Hess B, Kutzner C, van der Spoel D, Lindahl E. Journal of Chemical Theory and Computation. 2008; 4:435.
30. Yang DF, Wilde CP, Morin M. Langmuir. 1996; 12:6570.
31. Arihara K, Ariga T, Takashima N, Arihara K, Okajima T, Kitamura F, Tokuda K, Ohsaka T. Physical Chemistry Chemical Physics. 2003; 5:3758.
32. Kakiuchi T, Usui H, Hobara D, Yamamoto M. Langmuir. 2002; 18:5231.
33. Iwami Y, Hobara D, Yamamoto M, Kakiuchi T. Journal of Electroanalytical Chemistry. 2004; 564:77.
34. Aguilar-Sanchez R, Su GJ, Homberger M, Simon U, Wandlowski T. The Journal of Physical Chemistry C. 2007; 111:17409.
35. Kunze J, Leitch J, Schwan AL, Faragher RJ, Naumann R, Schiller S, Knoll W, Dutcher JR, Lipkowski J. Langmuir. 2006; 22:5509. [PubMed: 16732685]
36. Torrelles X, Vericat C, Vela ME, Fonticelli MH, Daza Millone MA, Felici R, Lee T-L, Zegenhagen J, Muñoz G, Martín-Gago JA, Salvarezza RC. The Journal of Physical Chemistry B. 2006; 110:5586. [PubMed: 16539501]
37. O'Dwyer C, Lavayen V, Fuenzalida D, Lozano H, Ana MAS, Benavente E, González G, Sotomayor Torres CM. Small. 2008; 4:990. [PubMed: 18535992]
38. Rabolt JF, Burns FC, Schlotter NE, Swalen JD. The Journal of Chemical Physics. 1983; 78:946.
39. Snyder RG, Hsu SL, Krimm S. Spectrochimica Acta Part A: Molecular Spectroscopy. 1978; 34:395.

40. Porter MD, Bright TB, Allara DL, Chidsey CED. Journal of the American Chemical Society. 1987; 109:3559.
41. Yamada R, Uosaki K. Langmuir. 1998; 14:855.
42. Widrig CA, Chung C, Porter MD. Journal of Electroanalytical Chemistry and Interfacial Electrochemistry. 1991; 310:335.
43. Ulman A, Eilers JE, Tillman N. Langmuir. 1989; 5:1147.
44. Ramírez P, Andreu R, Cuesta Á, Calzado CJ, Calvente JJ. Analytical Chemistry. 2007; 79:6473. [PubMed: 17676927]
45. Mulder WH, Calvente JJ, Andreu R. Langmuir. 2001; 17:3273.

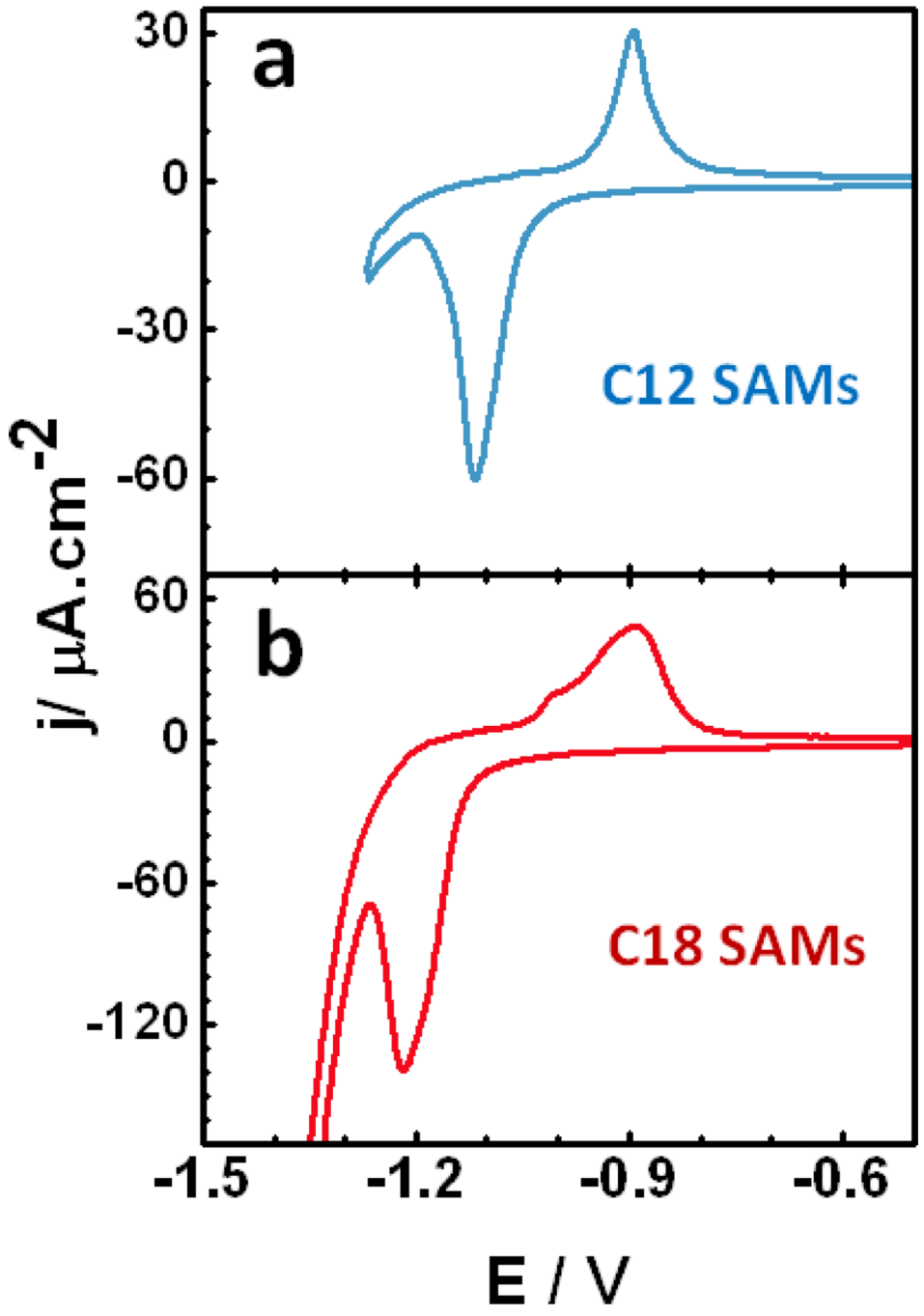

Figure 1.
Cyclic voltammograms of (a) dodecanethiol and (b) octadecanethiol SAMs on Au(111). Electrolyte: 0.1 M NaOH. Scan rate: 0.05 Vs^{-1}.

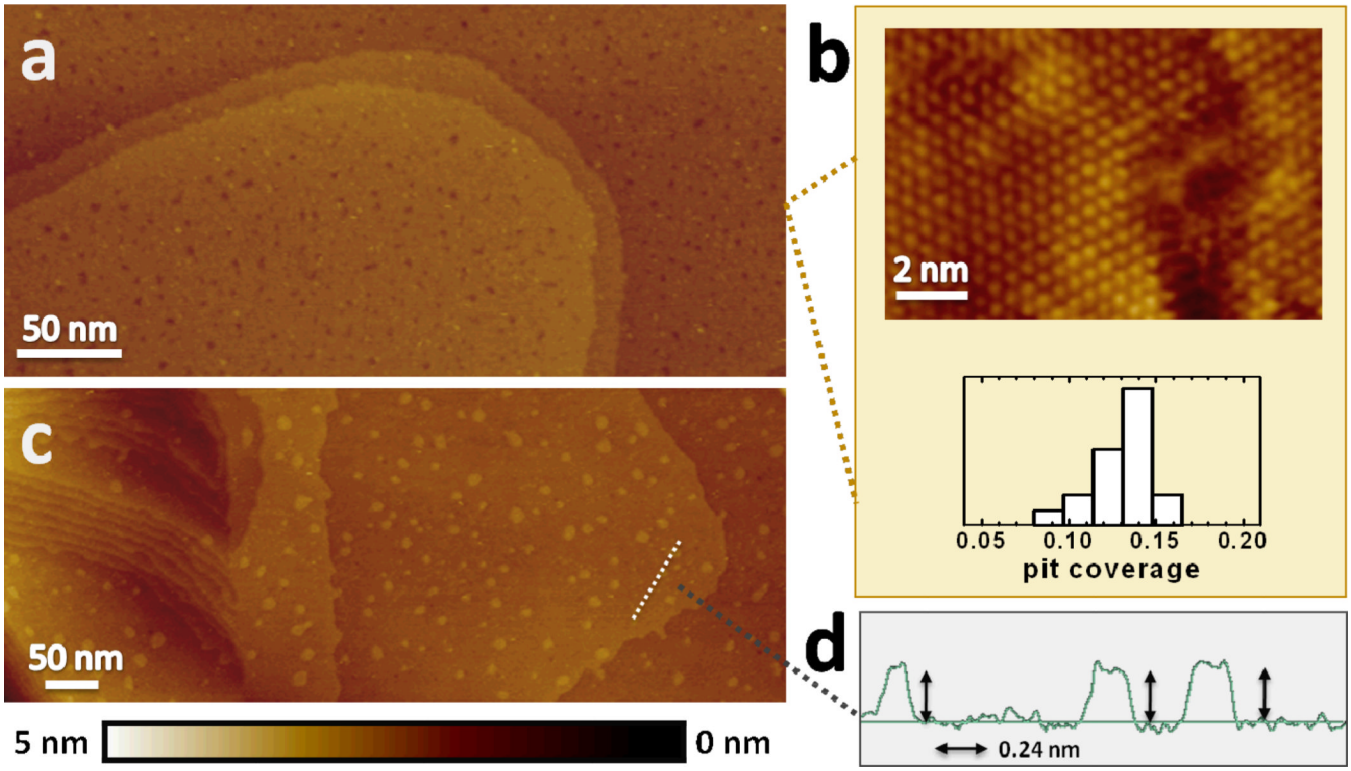

Figure 2.

In-air STM images of a dodecanethiol SAM on Au(111) taken (a) before and (c) after complete alkanethiol removal by electrodesorption cycles. (b) Upper: high resolution STM image showing the C12 √3×√3 R30° lattice on Au(111). Lower: histogram of the pit coverage distribution. (d) Cross section corresponding to the white line in (c) showing the height of the Au islands formed on the surface after complete C12 desorption.

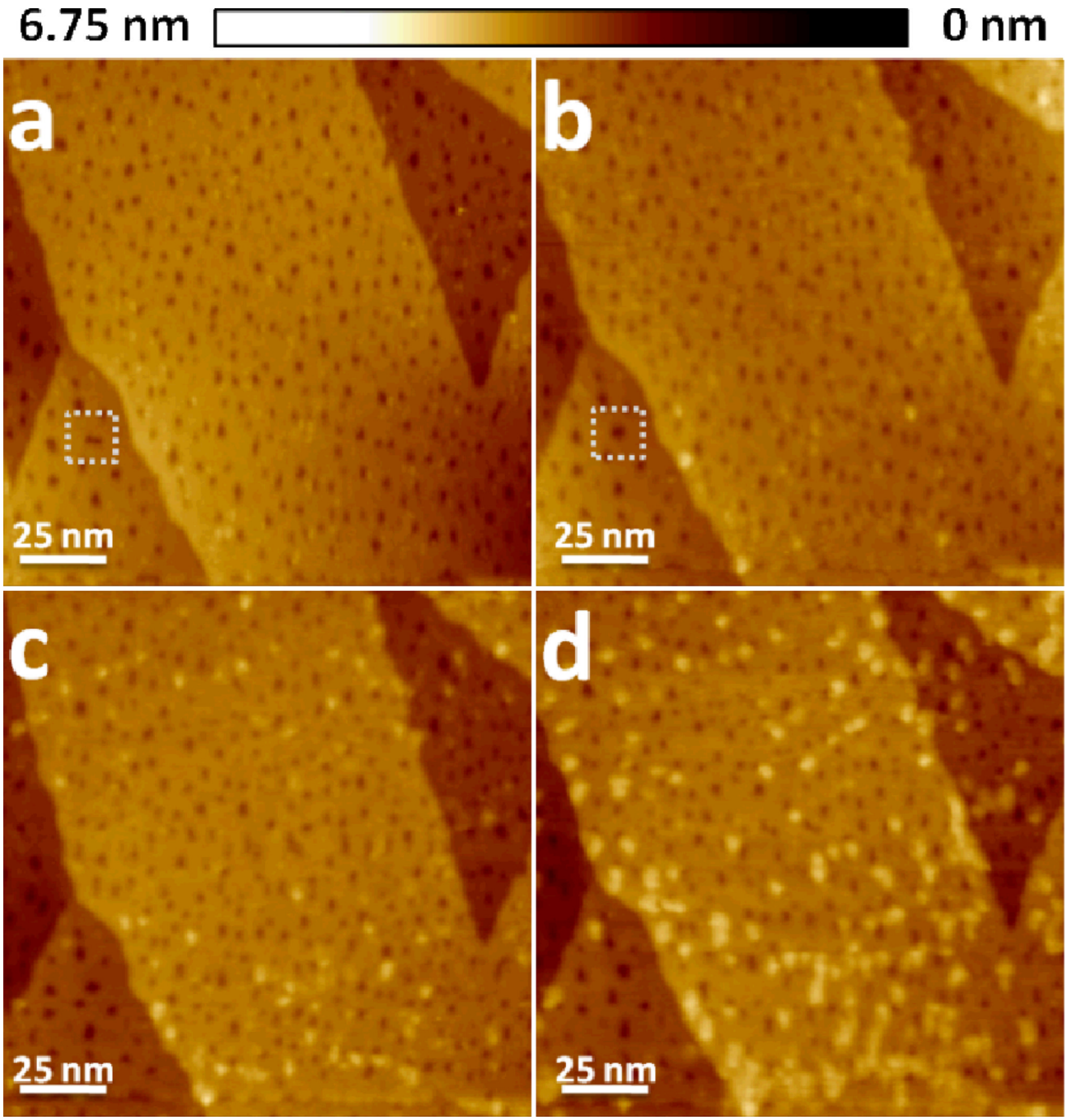

Figure 3.

ECSTM images as a function of the applied potential (E_s) for a dodecanethiol SAM on Au(111). All images show the characteristic gold vacancies. (a) E_s= −0.69 V. (b–d) E_s= −0.93 V. (b) t=0; (c) 3 min; (d) 6 min. Molecular agglomerates appear on the surface. In all cases E_{bias} = 750 mV and i_t= 2 nA.

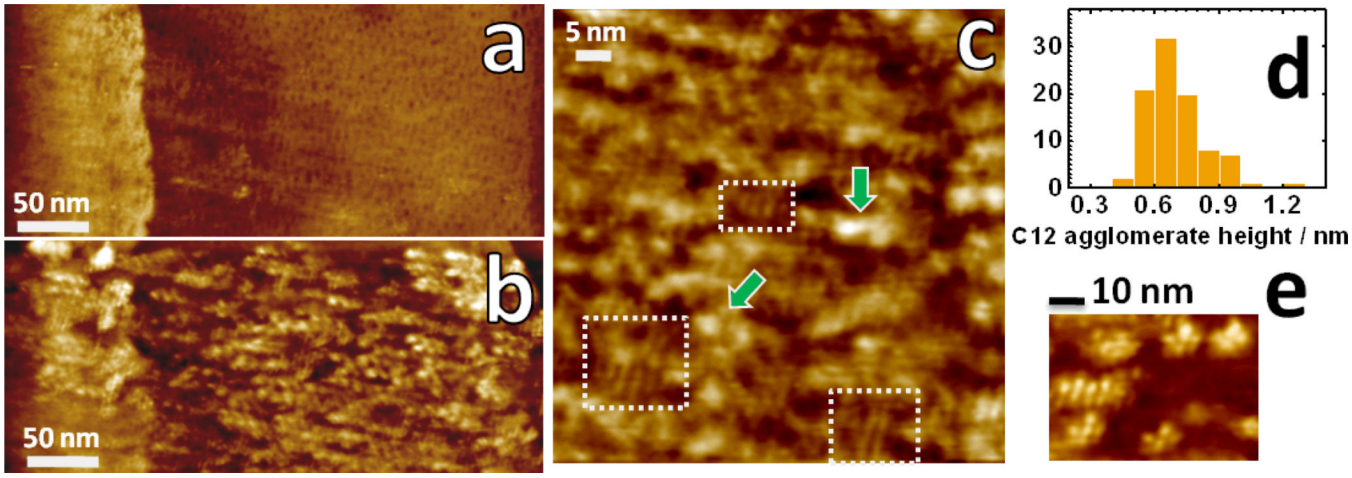

Figure 4.

ECSTM images and related data for a dodecanethiol SAM on Au(111). (a) E_s= −0.69 V. (b) E_s= −1.00 V. A larger amount of aggregates is formed on the surface. In both cases E_{bias} = 600 mV and i_t= 2.5 nA. (c) Higher resolution ECSTM image showing the lying down alkanethiol phase (white dotted rectangles) which coexists with the agglomerates (green arrows). (d) Height distribution of the bright spots. (e) High resolution ECSTM image of the agglomerates.

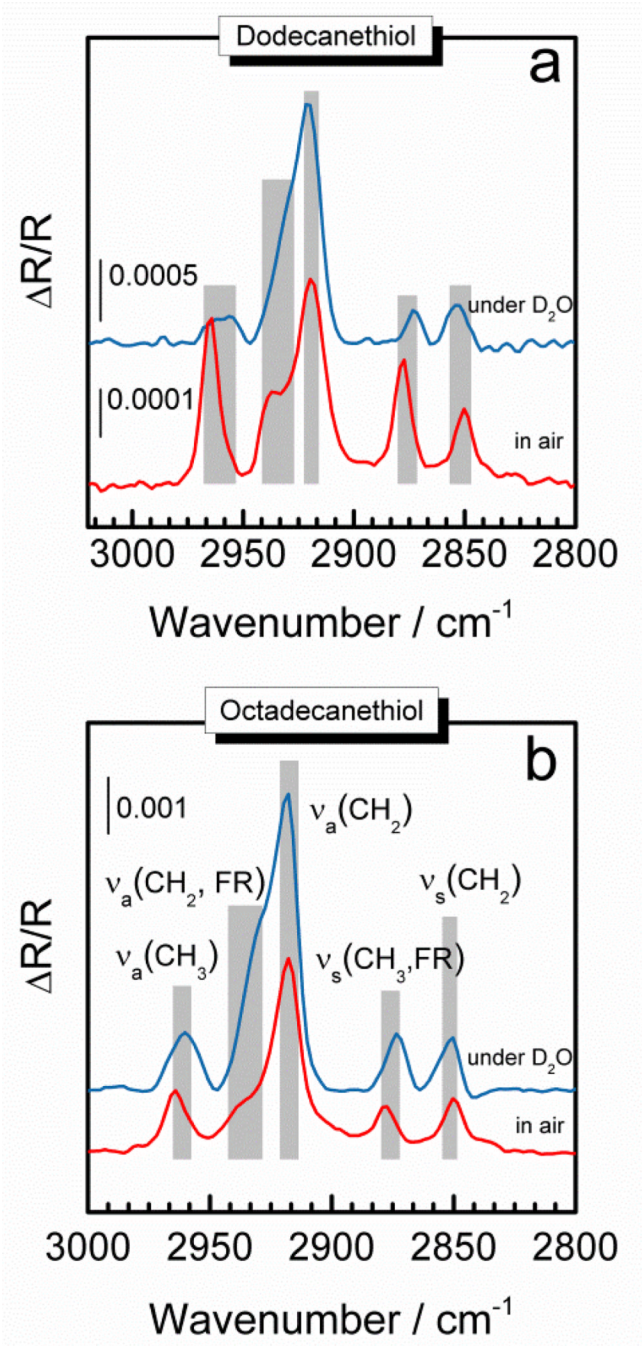

Figure 5.
PMIRRA spectra of (a) C12 and (b) C18 SAMs on gold in air and under 0.1M NaOH solution in deuterated water.

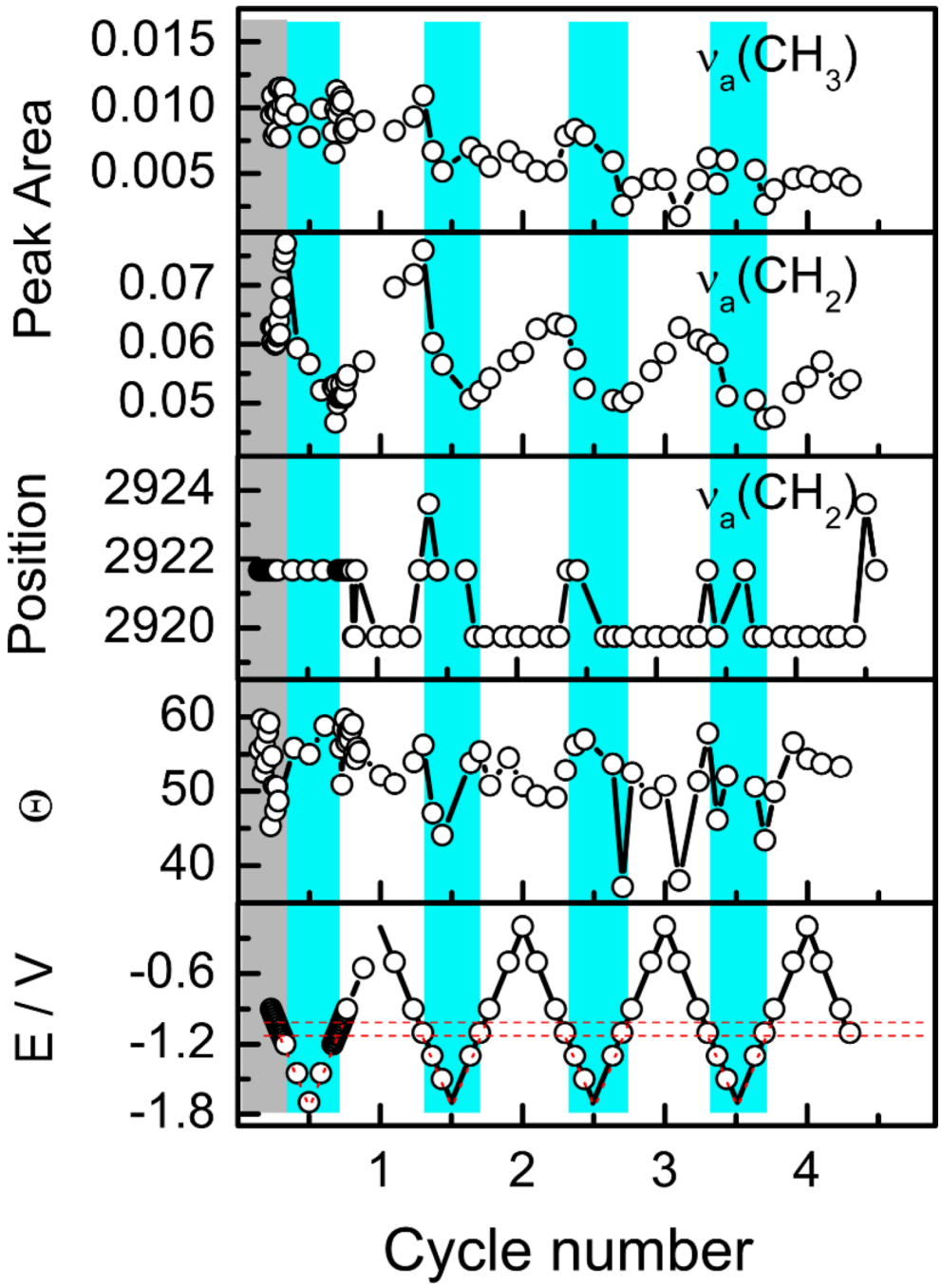

Figure 6.

PMIRRAS data for a C12 SAM on Au. From top to bottom, area of asymmetric CH_3 stretching peak ($\nu_a(CH_3)$), area of the asymmetric CH_2 stretching peak ($\nu_a(CH_2)$), position of the asymmetric CH_2 stretching peak ($\nu_a(CH_2)$) and calculated Θ angle from $\nu_a(CH_2)$ at different applied potentials as a function of the cycle number. The grey zone indicates the region studied in ECSTM experiments. The dotted purple lines in the bottom panel show the potentials considered for the onset of desorption and the beginning of readsorption in this experiment. The cyan zones correspond to the applied potentials between the onset of desorption and the beginning of readsorption of thiols.

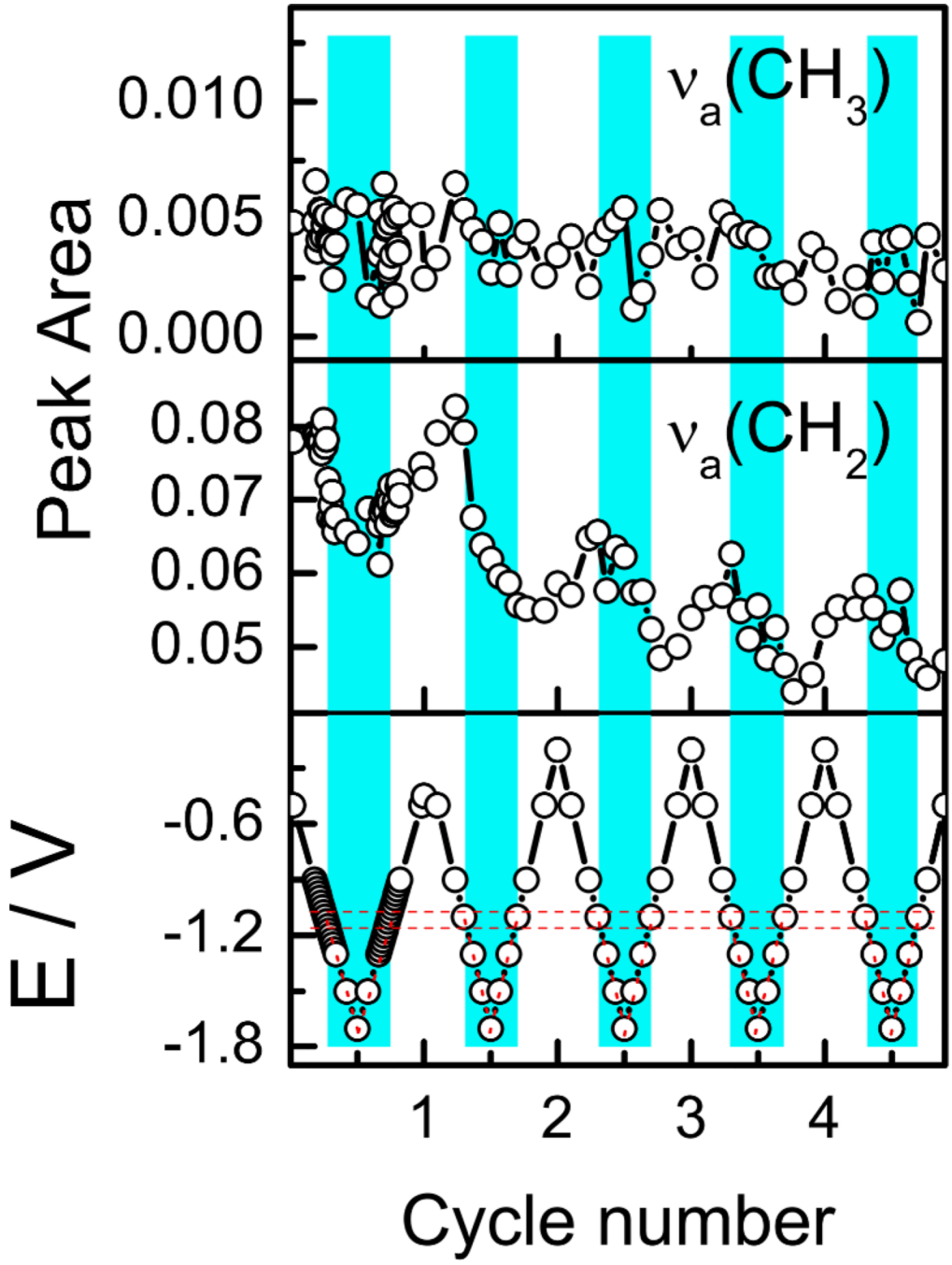

Figure 7.
PMIRRAS data for a C18 SAM on Au. From top to bottom, area of asymmetric CH_3 stretching peak ($\nu_a(CH_3)$) and area of the asymmetric CH_2 stretching peaks ($\nu_a(CH_2)$) at different applied potentials as a function of the cycle number. The dotted purple lines in the bottom panel show the potentials considered for the onset of desorption and the beginning of readsorption in this experiment. The cyan zones correspond to the applied potentials between the onset of desorption and the beginning of readsorption of thiols.

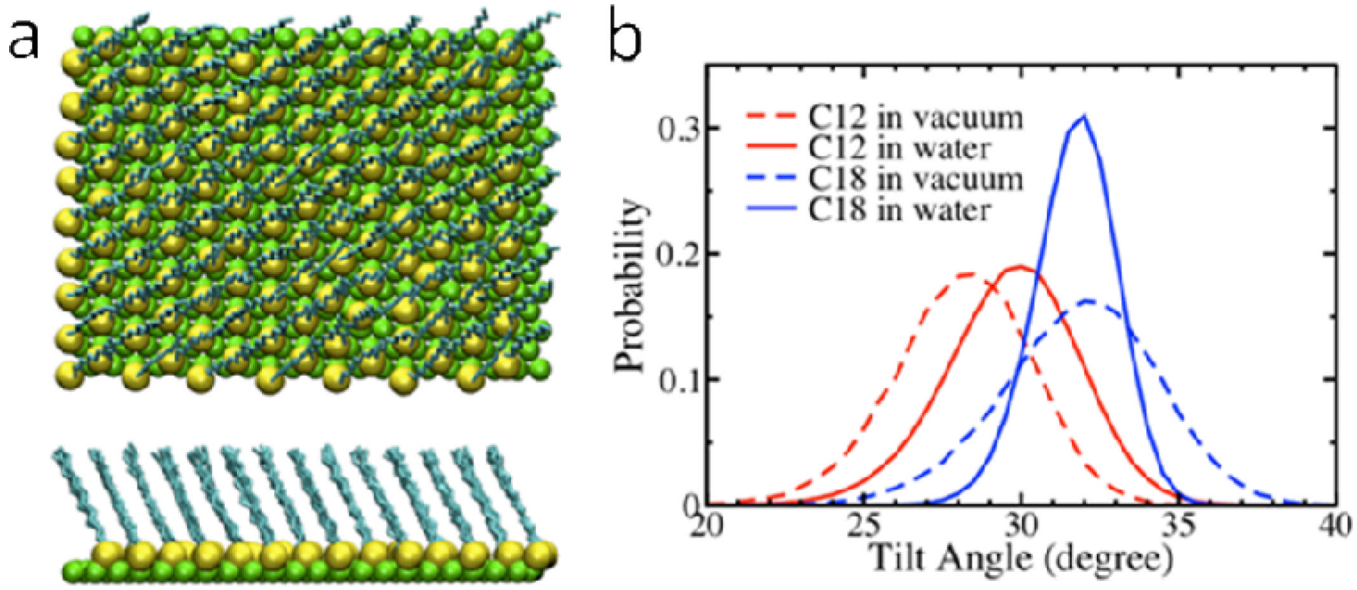

Figure 8.

(a) Top (above) and side (below) views of the C12 SAM (hydrocarbon segment in cyan and sulfur atom in yellow) on Au(111) substrate (green) after 5-ns MD simulation in vacuum. (b) The distributions of the tilt angles of the C12 and C18 alkanethiol SAMs in vacuum and in water

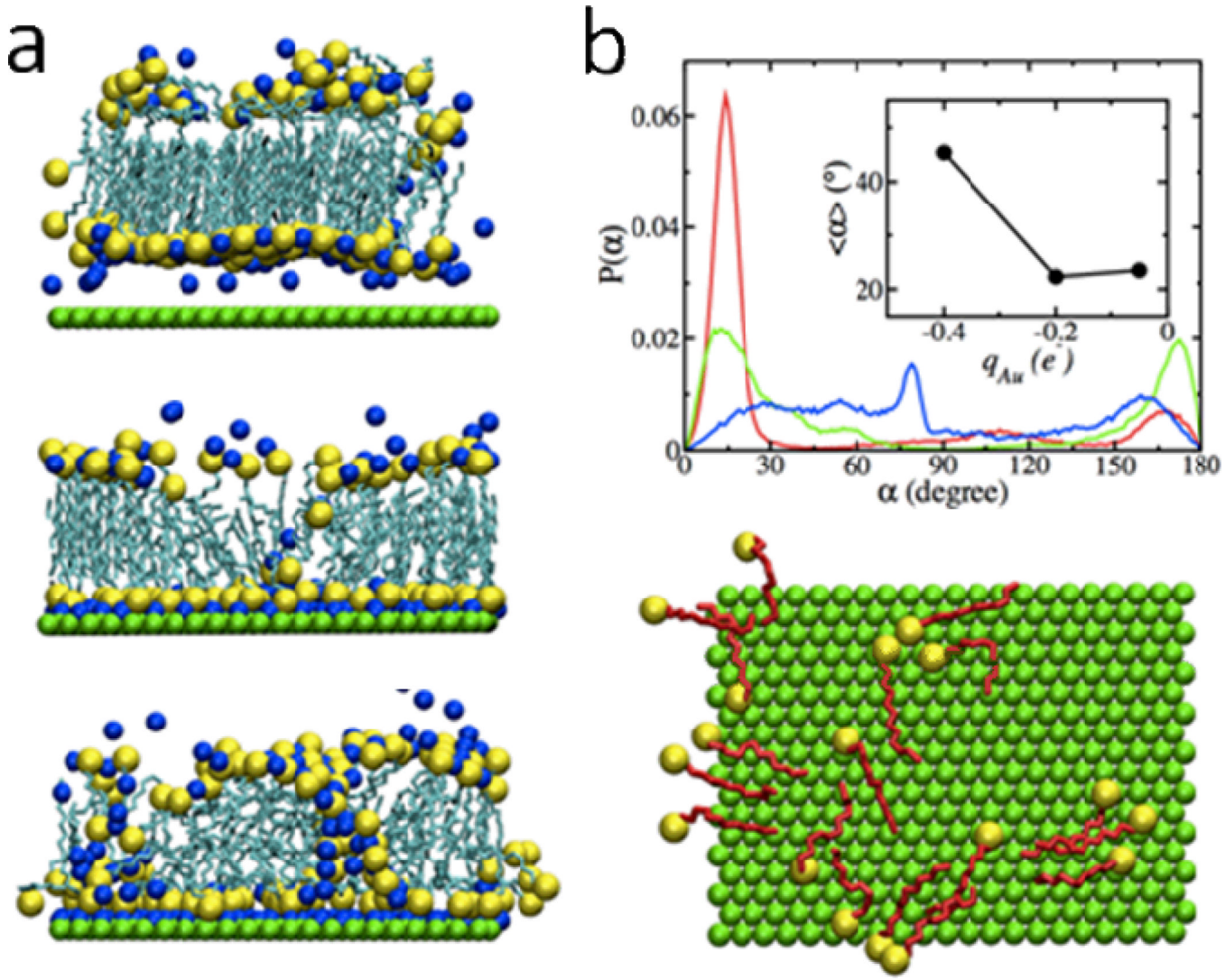

Figure 9.

(a) Final snapshots of the C12 SAM on Au(111) substrate with q_{Au} = −0.05 (top), −0.2 (middle), and −0.4 e^- (bottom) after the 10-ns simulations. Color scheme: Au (green), S (yellow), alkyl chain (cyan), Na^+ (blue). Water and Cl^- ions are not shown for clarity. On the lower right side, the lying-down phase of the alkanethiol molecules on the Au(111) substrate with q_{Au} = −0.4 e^- are shown in red color. The other alkanethiols and all the water and ions are not shown for clarity. (b) The tilt angle distributions, P(α), of the C12 alkanethiols near Au(111) substrate for the charges of q_{Au} = −0.05 (red), −0.2 (green), and −0.4 e^- (blue) on Au atom. (inset) The average tilt angle <α> of the C12 alkanethiol molecules from the simulations, equivalent to the average tilt angle derived from the PMIRRAS measurements

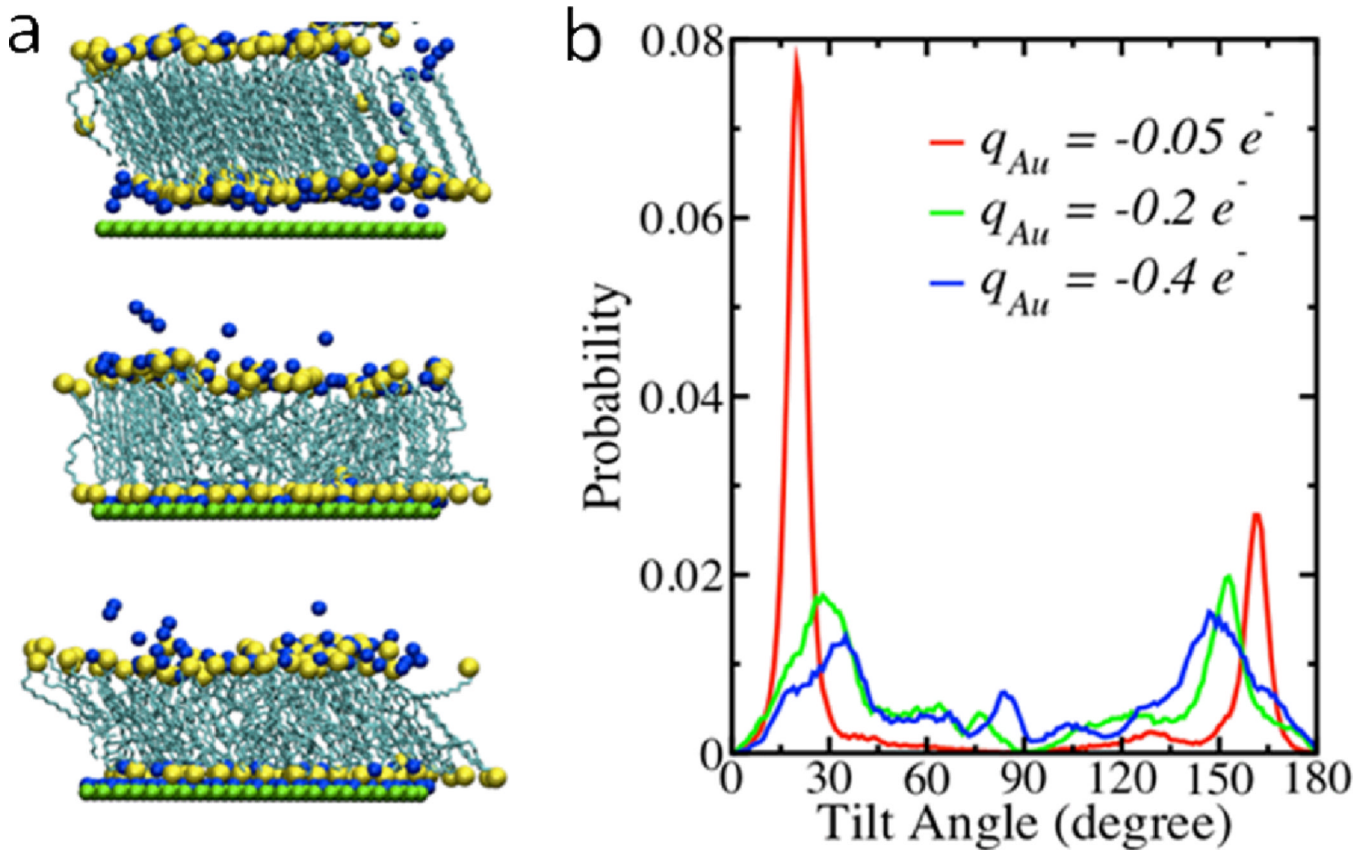

Figure 10.

(a) Snapshots of the C18 SAM. (b) The tilt angle distributions of the C18 alkanethiol molecules for different charges on the surface Au atoms on the Au(111) surface with q_{Au} = −0.05 (top), −0.2 (middle), and −0.4 e^- (bottom) at the end of the 10-ns MD simulations.